Available online at www.sciencedirect.com
ScienceDirect
Journal of Computational Physics 227 (2008) 4563–4588
JOURNAL OF COMPUTATIONAL PHYSICS
www.elsevier.com/locate/jcp

Multidimensional optimization of finite difference schemes for Computational Aeroacoustics

Adrian Sescu *, Ray Hixon, Abdollah A. Afjeh

MIME Department, University of Toledo, 2801 W Bancroft, MS 312, Toledo, OH 43606, United States

Received 20 August 2007; received in revised form 19 December 2007; accepted 10 January 2008
Available online 20 January 2008

Abstract

Because of the long propagation distances, Computational Aeroacoustics schemes must propagate the waves at the correct wave speeds and lower the isotropy error as much as possible. The spatial differencing schemes are most frequently analyzed and optimized for one-dimensional test cases. Therefore, in multidimensional problems such optimized schemes may not have isotropic behavior. In this work, optimized finite difference schemes for multidimensional Computational Aeroacoustics are derived which are designed to have improved isotropy compared to existing schemes. The derivation is performed based on both Taylor series expansion and Fourier analysis. Various explicit centered finite difference schemes and the associated boundary stencils have been derived and analyzed. The isotropy corrector factor, a parameter of the schemes, can be determined by minimizing the integrated error between the phase or group velocities on different spatial directions. The order of accuracy of the optimized schemes is the same as that of the classical schemes, the advantage being in reducing the isotropy error. The present schemes are restricted to equally-spaced Cartesian grids, so the generalized curvilinear transformation method and Cartesian grid methods are good candidates. The optimized schemes are tested by solving various multidimensional problems of Aeroacoustics.

Keywords: Finite difference methods; Isotropy error; Aeroacoustics

1. Introduction

The goal of Computational Aeroacoustics is the accurate prediction of unsteady flow and noise (see, e.g. [5,14,21]). To achieve this goal, high accuracy time marching schemes (see, e.g. [7,11]) are combined with optimized spatial differencing schemes (see, e.g. [1,2,6,9,13,15,16,22]) and proper boundary conditions (see, e.g. [5,8,10,23]). As the computational schemes become more robust, these methods are being applied to more realistic and complex flow geometries, using multidimensional curvilinear coordinate grids. Because the spatial differencing schemes are analyzed and optimized for one-dimensional test cases, in multidimensional problems

* Corresponding author. Tel.: +1 419 530 6066; fax: +1 419 530 8206.
E-mail address: adrian.sescu@utoledo.edu (A. Sescu).

0021-9991/$ - see front matter © 2008 Elsevier Inc. All rights reserved.
doi:10.1016/j.jcp.2008.01.008

they may not have isotropic behavior. For accurate numerical simulations of wave propagation in multidimensions the isotropy error is as important as the other types of errors.

The optimization of the centered spatial differencing schemes in terms of lowering the dispersion error especially for Computational Aeroacoustics, Large Eddy Simulations and Direct Numerical Simulations is an actual field of research. Among others, there were two fundamental papers, Lele [15] and Tam and Webb [22], that revolutionized this field, the former concerning with the optimization of the compact schemes and the latter with the optimization of the explicit schemes (the so-called dispersion-relation-preserving, DRP, schemes), respectively. Since these two papers have appeared in the Aeroacoustics community a series of other proposals have entered in line. Kim and Lee [13] performed an analytic optimization of the compact finite difference schemes. They showed that an analytic optimization produces the maximum spatial resolution characteristics of the compact finite difference approximation in the evaluation of the spatial finite derivatives. Li [16] has proposed new wavenumber-extended high-order upwind-biased schemes up to 11th-order by means of Fourier analysis. He showed that both the upwind-biased scheme of order $2N-1$ and the corresponding centered differencing scheme of order $2N$ have the same dispersion characteristics. Mahesh [18] derived a family of compact finite difference schemes for the spatial derivatives in the Navier–Stokes equation based on Hermite interpolation. He simultaneously solved for the first and second derivatives getting higher-order of accuracy and better spectral resolution. Hixon [6] derived prefactored high-order compact schemes which use three-point stencils and returns up to eighth-order accuracy. His schemes combine the tridiagonal compact formulation with the optimized split derivative operators of an explicit MacCormack type scheme. The tridiagonal matrix inversion was avoided by using bidiagonal matrices for the forward and backward operators. The optimization of Hixon's [6] schemes in terms of dispersion error was performed by Ashcroft and Zhang [1] who used Fourier analysis to select the coefficients of the biased operators such that the dispersion characteristics match those of the original centered compact scheme and their numerical wavenumbers have equal and opposite imaginary components.

All of the above optimizations were performed in one-dimensional space and they may suffer from the isotropy error (or numerical anisotropy) in multidimensions. It is known, for example, that the DRP scheme of Tam and Webb [22] has a particular value of the number of points per wavelength that makes the numerical wavenumber exactly equal to the analytical wavenumber. For a two-dimensional problem solved on a Cartesian grid this is true along the grid lines directions, and no longer true along the other directions. This undoubtedly occurs due to the numerical anisotropy, and this work proposes a way to deal with it, being an extension to three-dimensions of a previous attempt, [19,20]. An extended analysis of the isotropy error was performed by Vichnevetsky [25] who solved the two-dimensional wave equation using two different schemes for the Laplacian operator, and averaged the two solutions. Considerable improvement of the isotropy of wave propagation was obtained based on variation of the weighted average. Slightly the same idea was considered by Trefethen [24] who used the leap frog scheme to solve the wave equation in two-dimensions. Zingg and Lomax [27] performed optimizations of finite difference schemes applied on regular triangular grids, which give six neighbor points for a given node. Tam and Webb [23] proposed an anisotropy correction for Helmholtz equation; they found the anisotropy correction factor applicable to all noise radiation problems irrespective of the complexity of the noise sources. Lin and Sheu [17] used the idea of dispersion-relation-preserving (DRP) of Tam and Webb [22] in two-dimensions to optimize the first-order spatial derivative terms of a model equation that resembles the incompressible Navier–Stokes momentum equation. They approximated the derivative in the nine-point grid system resulting in nine unknown coefficients. Eight of them were determined by employing Taylor series expansions, and the remaining one was determined by requiring that the two-dimensional numerical dispersion relation is the same as the exact dispersion relation. Their method would be arduous for a possible generalization to higher-order schemes or to more than two spatial dimensions. The optimization developed in this paper can be easily applied to any explicit finite difference scheme regardless of the order of accuracy. In addition, Lin and Sheu have included the central grid point in the scheme which would generally result in numerical dissipation error. The optimized schemes developed here retain the characteristics of the classical schemes in terms of the numerical dissipation. Xiao et al. [26] introduced the concept of arbitrary order Taylor finite difference (TFD) and window finite difference (WFD) for the numerical solution of Maxwell's equations.

They did a dispersion and isotropy error analysis as a function of some factors, such as the number of cells per the exact wavelength (CPW) or Courant number. Explicit high-order finite difference schemes that use a large number of points may improve the isotropy of wave propagation, but they also may have serious issues at the boundaries. Many authors (see, e.g. [3,15] or [16]), in their works, have given information about the isotropy error of various optimized schemes, but few of them have attempted to perform optimization in terms of isotropy error. Such optimization is needed, for example, in some problems of Computational Aeroacoustics in which the propagation of sound for long distances is investigated.

As a preamble, in Fig. 1 the Gaussian impulse propagating from the origin is depicted, computed using second order classical schemes (Fig. 1(a)) and optimized corresponding schemes (Fig. 1(b)) derived later in this work. The waves were computed by solving the Linearized Euler Equation in two-dimensions with a grid spacing of 2 for both directions. For now, only the isotropy error is important; the figure may show spurious waves or unresolved zones, but they are not important in this context. One-dimensional optimizations for the existing schemes performed in the x-direction (horizontal direction) using classical schemes would not work well on other directions due to anisotropy. The present work proposes a way to deal with this kind of problem. The need for optimizations in multidimensions would be well-motivated because most of the real problems are defined in multidimensional space.

The starting point of this work is based on the idea of weighted averaging applied before by Vichnevetsky [25], or Trefethen [24]. Instead of solving the equation twice, new optimized schemes are derived using the weighted averaging technique and the transformation matrix between two orthogonal or non-orthogonal bases. The averaging is applied between two or three schemes, representing, for example, the x derivative: one of them is the classical scheme taking into account only the points along the x-direction, and the other is a scheme that takes into account the derivatives along the $x = y$ and $x = -y$ in two-dimensions or the $x = y = z$, $x = y = -z$, $x = -y = -z$ and $x = -y = z$ directions in three-dimensions using the transformation matrices. Up to this point everything is discretized using Taylor series expansions because the new schemes are supposed to be linear combinations of classical finite difference schemes. Therefore, in terms of truncation error analysis, the proposed optimized schemes are shown to have the same order of accuracy as the corresponding classical schemes. Using Fourier analysis, their advantage is revealed in terms of isotropy error: compared to classical schemes, they have improved isotropy. The isotropy effectiveness of the optimized schemes is controlled by a parameter hereafter called isotropy corrector factor (referred to as ICF) which can be found based on requiring that the phase or group velocities be the same in specified directions. Thus, the numerical dispersion relation relating the numerical wave numbers in the x, y and z directions and the frequency must transport the waves (or wave packets) with the same phase or group velocities in all directions. To fulfill this requirement, the integrated error between the phase or group velocities, for example, in the x and $x = y = z$ directions is minimized with respect to ICF. Boundary schemes are also derived; the numerical wave number in this case has both real and imaginary parts, corresponding to dispersion and dissipation, respec-

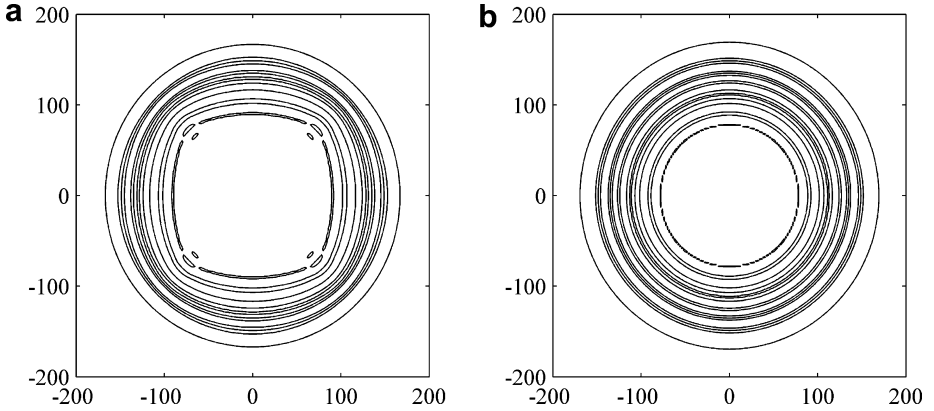

Fig. 1. Two-dimensional wave computed using classical second order schemes (a) and optimized second order schemes (b).

tively. Special care must be taken at the corner and near the corner where different optimized schemes are derived.

The organization of the paper is as follows. In Section 2, the dispersion relation for the Linearized Euler Equations (LEE) in three-dimensions is determined. In Section 3, a detailed procedure of deriving the optimized schemes and finding ICF is presented. In Section 4, a problem from the First Computational Aeroacustics Workshop [2] is considered and the numerical results obtained using the optimized schemes are compared to analytical solutions. The anisotropy correction is revealed by superposing the front waves from different radial directions. The effect of the grid stretching is also analyzed and discussed. Concluding remarks are given in Section 5. The Taylor series expansions for the second, fourth and sixth order optimized two-dimensional centered schemes and the second order optimized three-dimensional centered scheme are presented in the Appendix.

2. Dispersion relation of the linearized euler equation

Wave propagation is an inherent feature of the solutions of hyperbolic equations. In multidimensional space most of the waves or wave packets (for example, the sound wave) are propagating in all directions with the same phase or group velocity, respectively: this characteristic is called isotropy of wave propagation. Consider waves in a three-dimensional, uniform, isentropic, subsonic flow $(\bar{u},0,0)$ along the x-direction of a compressible fluid. For small perturbations in the density and the velocity components, we may linearize and nondimensionalize the Euler equations of gas dynamics so that we get the Linearized Euler Equations (LEE)

$$\frac{\partial Q}{\partial t}+\frac{\partial E}{\partial x}+\frac{\partial F}{\partial y}+\frac{\partial G}{\partial z}=S, \tag{1}$$

where

$$Q=\begin{bmatrix}\rho'\\ u'\\ v'\\ w'\\ p'\end{bmatrix},\quad E=\begin{bmatrix}M_x\rho'+u'\\ M_xu'+p'\\ M_xv'\\ M_xw'\\ M_xp'+u'\end{bmatrix},\quad F=\begin{bmatrix}v'\\ 0\\ p'\\ 0\\ v'\end{bmatrix},\quad G=\begin{bmatrix}w'\\ 0\\ 0\\ p'\\ w'\end{bmatrix} \tag{2}$$

ρ',u',v',w' and p' are the perturbations of density, x-component velocity, y-component velocity, z-component velocity and pressure, respectively. M_x is the x-component of Mach number determined using the mean velocity. The linearization is possible because the amplitudes of the perturbations are much smaller than the fluid mean properties.

The Fourier–Laplace transform and its inverse of velocity perturbation u', for example, are defined by

$$\tilde{u}(k_1,k_2,k_3,\omega)=\frac{1}{(2\pi)^3}\int_0^\infty\int\int\int_{-\infty}^{\infty}u'(x,y,z,t)\cdot e^{-i(k_1x+k_2y+k_3z-\omega t)}\,dx\,dy\,dz\,dt \tag{3}$$

and

$$u'(x,y,z,t)=\int_\Gamma\int\int\int_{-\infty}^{\infty}\tilde{u}(k_1,k_2,k_3,\omega)\cdot e^{i(k_1x+k_2y+k_3z-\omega t)}\,dk_1\,dk_2\,dk_3\,d\omega, \tag{4}$$

where Γ is a line parallel to the real axis in the complex ω-plane above all poles and singularities of the integrand [22]. The components of the wave number are denoted by k_1, k_2 and k_3, and the frequency is denoted by ω. It is assumed for the moment that the source term S in Eq. (1) is zero. Applying the Fourier-Laplace transform to Eq. (1), the next eigenvalue-problem is obtained:

$$A\widetilde{Q}=\widetilde{G}, \tag{5}$$

where $\widetilde{G}$ may result from the transformation of the initial conditions. The matrix A in Eq. (5) is given by

$$A = \begin{bmatrix} \omega - k_1 M_x & -k_1 & -k_2 & -k_3 & 0 \\ 0 & \omega - k_1 M_x & 0 & 0 & -k_1 \\ 0 & 0 & \omega - k_1 M_x & 0 & -k_2 \\ 0 & 0 & 0 & \omega - k_1 M_x & -k_3 \\ 0 & -k_1 & -k_2 & -k_3 & \omega - k_1 M_x \end{bmatrix}, \tag{6}$$

and it is easy to show that its eigenvalues are

$$\begin{aligned} \lambda_1 &= \lambda_2 = \lambda_3 = \omega - k_1 M_x \\ \lambda_4 &= (\omega - k_1 M_x) + \sqrt{k_1^2 + k_2^2 + k_3^2} \\ \lambda_5 &= (\omega - k_1 M_x) - \sqrt{k_1^2 + k_2^2 + k_3^2} \end{aligned} \tag{7}$$

The dispersion relations of the waves (entropy, vorticity or acoustic waves) are determined by making the determinant of the matrix A zero. This occurs when any of its eigenvalues is zero. The first, the second and the third eigenvalues (λ_1, λ_2 and λ_3) correspond to entropy and vorticity waves, whereas the fourth and the fifth eigenvalues (λ_4 and λ_5) correspond to acoustic waves, respectively. The dispersion relation for the acoustic waves propagating in all directions is given by equalizing the product of λ_4 and λ_5 to zero.

$$\lambda_4 \lambda_5 = (\omega - k_1 M)^2 - (k_1^2 + k_2^2 + k_3^2) = 0. \tag{8}$$

Looking at λ_1, λ_2 and λ_3 in Eq. (7) it is obvious that the entropy and vorticity waves vanish for a stationary mean flow. The acoustic waves, however, still persist and their dispersion relation becomes

$$\omega^2 - (k_1^2 + k_2^2 + k_3^2) = 0. \tag{9}$$

Following the same procedure the dispersion relation for the two-dimensional case is given by

$$\omega^2 - (k_1^2 + k_2^2) = 0. \tag{10}$$

The dispersion relation (10) represents the equation of a cone in wave number-frequency space. It is obvious that Eq. (9) or (10) represents the dispersion relation for the three-dimensional or two-dimensional wave equation, respectively. This is the case because, for a stationary mean flow, after some manipulations, LEE becomes the wave equation. Without loss of generality, Eq. (9) or (10) will be considered in the next sections for the derivation of the optimized schemes.

3. The derivation of the optimized schemes

Due to the grid, when using finite difference schemes the isotropy error affects the wave propagation. The one-dimensional optimization of the finite difference schemes is not able to fully correct the anisotropy due to the grid; the improvement of isotropy of the wave propagation would be possible if very high-resolution finite difference schemes are used, or if the grid is sufficiently dense. The former possibility requires special care at the boundary, whereas the latter is computationally expensive. Therefore, a need for performing optimizations of finite difference schemes in multidimensions becomes justified. It is also particular for finite difference methods that the derivative along one direction in multidimensional space is calculated taking into account only the points along that direction. Because the distance between the points do not tend to zero (as the definition of the derivative requires), information about the other directions is missing. The present paper proposes a way to derive finite difference schemes in multidimensions that use information from points from more than one direction. Next, the procedure of deriving the optimized schemes in two and three-dimensions is presented.

3.1. Centered second order optimized schemes for two-dimensions

An equally-spaced two-dimensional Cartesian grid is considered with i index on the x-direction and j index on the y-direction. Most of the multidimensional computations based on finite difference schemes are

performed using body-fitted generalized curvilinear transformation which maps the physical domain onto the computational domain. Therefore, the hypothesis that $\Delta x = \Delta y$ which can be valid in the computational domain can be considered. Two orthogonal bases are considered, one (xOy) related to Cartesian grid directions and the other ($x'Oy'$) positioned at 45° with respect to the first, so that its axes passes through the grid points. The transformation matrix, Eq. (11), between these two orthogonal bases is used to derive the optimized schemes.

$$\begin{bmatrix} x' \\ y' \end{bmatrix} = \begin{bmatrix} \cos(\alpha) & \sin(\alpha) \\ -\sin(\alpha) & \cos(\alpha) \end{bmatrix} \cdot \begin{bmatrix} x \\ y \end{bmatrix}, \tag{11}$$

where α is the angle between x and x' axes (45° in this case). The relation between the derivatives of a function $u(x,y)$ based on Eq. (11) is

$$\begin{bmatrix} \frac{\partial u}{\partial x} \\ \frac{\partial u}{\partial y} \end{bmatrix} = \begin{bmatrix} \cos(\alpha) & -\sin(\alpha) \\ \sin(\alpha) & \cos(\alpha) \end{bmatrix} \cdot \begin{bmatrix} \frac{\partial u}{\partial x'} \\ \frac{\partial u}{\partial y'} \end{bmatrix}. \tag{12}$$

Using centered second order finite difference schemes for the x' and y' derivatives in Eq. (12), the approximation of the x derivative can be written:

$$\left(\frac{\partial u}{\partial x}\right)_{i,j} = \frac{1}{2\sqrt{2}\Delta x}[\cos(\alpha)(u_{i+1,j+1} - u_{i-1,j-1}) - \sin(\alpha)(u_{i-1,j+1} - u_{i+1,j-1})]. \tag{13}$$

The usual centered finite difference scheme using points along the x-direction is

$$\left(\frac{\partial u}{\partial x}\right)_{i,j} = \frac{1}{2\Delta x}[u_{i+1,j} - u_{i-1,j}]. \tag{14}$$

Averaging the scheme in Eq. (13) with the classical scheme in Eq. (14), and taking $\alpha = 45°$ results in

$$\left(\frac{\partial u}{\partial x}\right)_{i,j} = \frac{1}{2\Delta x(1+\beta)}\left[u_{i+1,j} - u_{i-1,j} + \frac{\beta}{2}(u_{i+1,j+1} - u_{i-1,j-1} + u_{i+1,j-1} - u_{i-1,j+1})\right]. \tag{15}$$

The parameter β represents the weighted average and will be called isotropy corrector factor (ICF). As β becomes zero the optimized scheme, Eq. (15), tends to the classical scheme, Eq. (14). The points used by the classical and optimized schemes are shown in Fig. 2.

Following the same idea, the approximation for the y derivative is

$$\left(\frac{\partial u}{\partial y}\right)_{i,j} = \frac{1}{2\Delta y(1+\beta)}\left[u_{i,j+1} - u_{i,j+1} + \frac{\beta}{2}(u_{i+1,j+1} - u_{i-1,j-1} + u_{i-1,j+1} - u_{i+1,j-1})\right]. \tag{16}$$

The Fourier transform applied to the above schemes approximating the x and y derivatives, Eqs. (15) and (16), gives the numerical wave numbers:

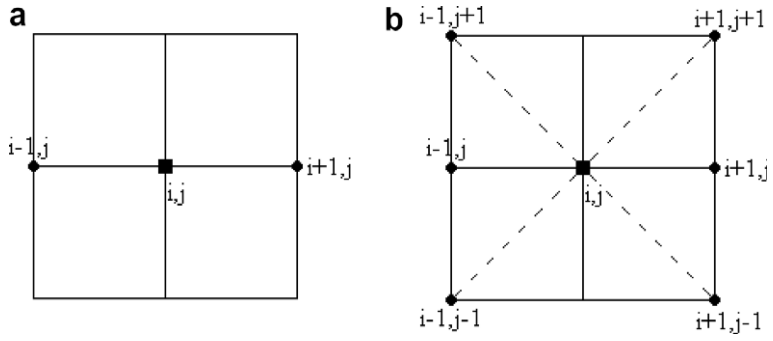

Fig. 2. Points used by classical (a) and optimized (b) centered second order approximating the x derivative.

$$(k_1\Delta x)^*_{\text{opt}} = \frac{1}{(1+\beta)}\left[\sin(k_1\Delta x) + \frac{\beta}{2}(\sin(k_1\Delta x + k_2\Delta y) + \sin(k_1\Delta x - k_2\Delta y))\right] \tag{17}$$

for the x derivative and

$$(k_2\Delta y)^*_{\text{opt}} = \frac{1}{(1+\beta)}\left[\sin(k_2\Delta y) + \frac{\beta}{2}(\sin(k_1\Delta x + k_2\Delta y) - \sin(k_1\Delta x - k_2\Delta y))\right] \tag{18}$$

for the y derivative.

Thus, according to Eq. (10), and assuming that the time integration is free of numerical dissipation and dispersion, the numerical dispersion relation using the optimized schemes is

$$\omega^2 - [(k_1\Delta x)^{*2}_{opt} + (k_2\Delta y)^{*2}_{opt}] = 0. \tag{19}$$

The surfaces of the numerical dispersion relations corresponding to classical and optimized second order schemes in wavenumber–frequency space are given in Fig. 3; ICF magnitude was considered 0.51 (in Section 3 the method for the determination of ICF is presented). Surfaces in Fig. 3 are approximations of the exact dispersion relation surface which represent a cone.

In Section 3.5. ICF will be determined by requiring that the phase or group velocities be the same on some specified direction. Next, the corresponding three-dimensional optimized schemes are derived following the same idea.

3.2. Centered second order optimized schemes for three-dimensions

A three-dimensional Cartesian grid is considered with i index on the x-direction, j index on the y-direction and k index on the z-direction (the origin of the three-dimensional reference frame is denoted by O). The hypothesis $\Delta x = \Delta y = \Delta z$ is again considered. Suppose that the x derivative is to be approximated. In addition, four reference frames in two-dimensions are considered (see Fig. 4): the first is orthogonal and has the axes aligned with the x and $y = z$ directions; the second is also orthogonal and has the axes aligned with the x and $y = -z$ directions; the third, is non-orthogonal and its axes are aligned with the $x = y = z$ and $x = -y = -z$ directions; and the fourth, is non-orthogonal and its axes are aligned with the $x = -y = z$ and $x = y = -z$ directions. (see Fig. 4) The matrix that relates an orthogonal basis (for example, xOy_1) with a non-orthogonal basis (for example, x_3Oy_3) is given by

$$A = \begin{bmatrix} \frac{\sqrt{3}}{2} & -\frac{\sqrt{6}}{4} \\ \frac{\sqrt{3}}{2} & \frac{\sqrt{6}}{4} \end{bmatrix}. \tag{20}$$

Using the transformation matrix, Eq. (20), the next relations between the derivatives taken in different bases result:

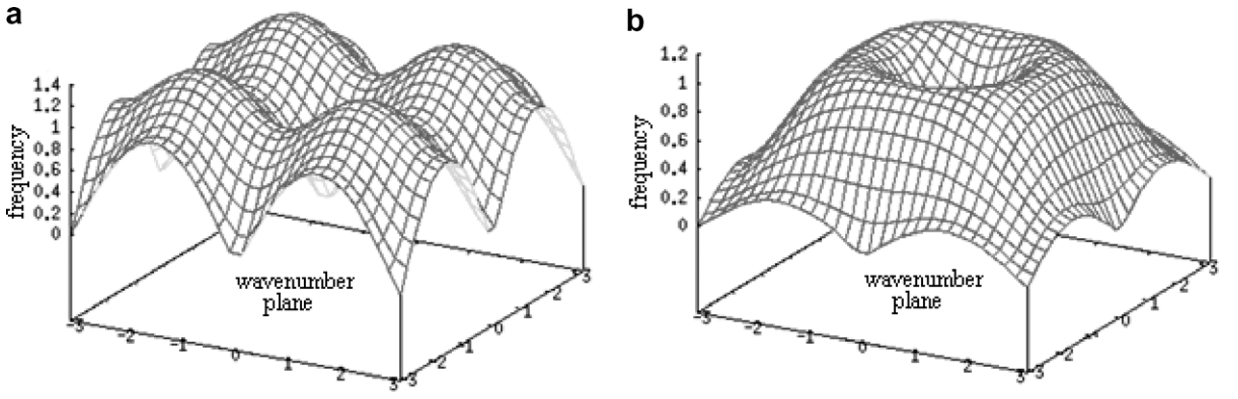

Fig. 3. Numerical dispersion relation surfaces using (a) second order classical schemes and (b) second order optimized schemes.

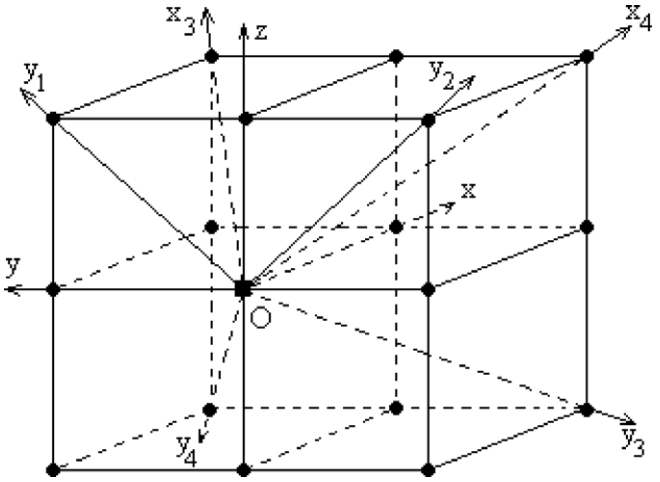

Fig. 4. The bases used for the derivation of the optimized three-dimensional difference schemes.

$$\left(\frac{\partial u}{\partial x}\right)_{i,j,k} = \frac{\sqrt{3}}{2}\left[\left(\frac{\partial u}{\partial x_3}\right)_{i,j,k} + \left(\frac{\partial u}{\partial y_3}\right)_{i,j,k}\right] \tag{21}$$

and

$$\left(\frac{\partial u}{\partial x}\right)_{i,j,k} = \frac{\sqrt{3}}{2}\left[\left(\frac{\partial u}{\partial x_4}\right)_{i,j,k} + \left(\frac{\partial u}{\partial y_4}\right)_{i,j,k}\right]. \tag{22}$$

Using the weighted averaging as in two-dimensional case in the previous section, the next scheme for the x derivative is obtained:

$$\left(\frac{\partial u}{\partial x}\right)_{i,j,k} = \frac{1}{2\Delta x(1+2\beta)}\left[u_{i+1,j,k} - u_{i-1,j,k} + \frac{\beta}{2}\left(u_{i+1,j+1,k+1} - u_{i-1,j-1,k-1} + u_{i+1,j-1,k+1} - u_{i-1,j+1,k-1} + u_{i+1,j+1,k-1} - u_{i-1,j-1,k+1} + u_{i+1,j-1,k-1} - u_{i-1,j+1,k+1}\right)\right]. \tag{23}$$

Eq. (23) was obtained by weighted averaging three terms representing finite difference schemes of the x derivative in three different bases: the corresponding weights are 1, β and β. It is supposed that two of the terms have the same weights, which means that their contributions are equivalent. Following the same idea, the approximations of the y and z derivative are

$$\left(\frac{\partial u}{\partial y}\right)_{i,j,k} = \frac{1}{2\Delta y(1+2\beta)}\left[u_{i,j+1,k} - u_{i,j-1,k} + \frac{\beta}{2}\left(u_{i+1,j+1,k+1} - u_{i-1,j-1,k-1} + u_{i-1,j+1,k+1} - u_{i+1,j-1,k-1} + u_{i+1,j+1,k-1} - u_{i-1,j-1,k+1} + u_{i-1,j+1,k-1} - u_{i+1,j-1,k+1}\right)\right], \tag{24}$$

$$\left(\frac{\partial u}{\partial z}\right)_{i,j,k} = \frac{1}{2\Delta z(1+2\beta)}\left[u_{i,j,k+1} - u_{i,j,k-1} + \frac{\beta}{2}\left(u_{i+1,j+1,k+1} - u_{i-1,j-1,k-1} + u_{i-1,j+1,k+1} - u_{i+1,j-1,k-1} + u_{i+1,j+1,k-1} - u_{i-1,j-1,k+1} + u_{i-1,j-1,k+1} - u_{i+1,j+1,k-1}\right)\right]. \tag{25}$$

The two-dimensional second order optimized schemes use 6 grid points instead of 2 (used by the classical second order schemes), and the three-dimensional second order optimized schemes use 10 grid points instead of 2. This involves slightly more computer time in running the code. Based on a Computational Aeroacoustics or Computational Fluid Dynamics solver which involves the numerical solution of either Euler or

Navier–Stokes equations on a Cartesian grid using Low-Dissipation and -Dispersion 4–6 Runge–Kutta scheme [11] or classical Runge–Kutta scheme as time-marching technique and classical filtering terms [12] up to 10th order, the clock time may be increased with approximately 7.5% by using two-dimensional optimized schemes and 10% by using three-dimensional optimized schemes.

3.3. Generalization

Following the same idea, higher-order centered optimized finite difference schemes can be derived. First, consider the general approximation of the first derivative by the $(N+1)$ point stencil for the x and y directions in two-dimensions

$$\left(\frac{\partial u}{\partial x}\right)_{i,j} = \frac{1}{\Delta x}\sum_{n=-N}^{N} a_n u_{i+n,j} \quad \text{and} \quad \left(\frac{\partial u}{\partial y}\right)_{i,j} = \frac{1}{\Delta y}\sum_{n=-N}^{N} a_n u_{i,j+n}, \tag{26}$$

and the general approximation of the first derivative by the $(N+1)$ point stencil for the x, y and z directions in three-dimensions,

$$\left(\frac{\partial u}{\partial x}\right)_{i,j,k} = \frac{1}{\Delta x}\sum_{n=-N}^{N} a_n u_{i+n,j,k}, \quad \left(\frac{\partial u}{\partial y}\right)_{i,j,k} = \frac{1}{\Delta y}\sum_{n=-N}^{N} a_n u_{i,j+n,k} \quad \text{and} \quad \left(\frac{\partial u}{\partial z}\right)_{i,j,k} = \frac{1}{\Delta y}\sum_{n=-N}^{N} a_n u_{i,j,k+n}. \tag{27}$$

The values of coefficients a_n in Eqs. (26) and (27) for several frequently used centered schemes are given in Table 1. The corresponding optimized schemes are determined in the same manner as before. Their general forms are

$$\left(\frac{\partial u}{\partial x}\right)_{i,j} = \frac{1}{\Delta x(1+\beta)}\sum_{n=-N}^{N} a_n\left[u_{i+n,j} + \frac{\beta}{2}\left(u_{i+n,j+n} + u_{i+n,j-n}\right)\right], \tag{28}$$

$$\left(\frac{\partial u}{\partial y}\right)_{i,j} = \frac{1}{\Delta y(1+\beta)}\sum_{n=-N}^{N} a_n\left[u_{i,j+n} + \frac{\beta}{2}\left(u_{i+n,j+n} + u_{i-n,j+n}\right)\right] \tag{29}$$

for two-dimensions and

$$\left(\frac{\partial u}{\partial x}\right)_{i,j,k} = \frac{1}{2\Delta x(1+2\beta)}\sum_{n=-N}^{N} a_n\left[u_{i+n,j,k} + \frac{\beta}{2}\left(u_{i+n,j+n,k+n} + u_{i-n,j+n,k+n} + u_{i-n,j-n,k+n} + u_{i-n,j+n,k-n}\right)\right], \tag{30}$$

$$\left(\frac{\partial u}{\partial y}\right)_{i,j,k} = \frac{1}{2\Delta y(1+2\beta)}\sum_{n=-N}^{N} a_n\left[u_{i,j+n,k} + \frac{\beta}{2}\left(u_{i+n,j+n,k+n} + u_{i+n,j-n,k-n} + u_{i-n,j-n,k+n} + u_{i+n,j-n,k+n}\right)\right], \tag{31}$$

$$\left(\frac{\partial u}{\partial z}\right)_{i,j,k} = \frac{1}{2\Delta z(1+2\beta)}\sum_{n=-N}^{N} a_n\left[u_{i,j,k+n} + \frac{\beta}{2}\left(u_{i+n,j+n,k+n} + u_{i-n,j+n,k-n} + u_{i+n,j-n,k-n} + u_{i+n,j+n,k-n}\right)\right] \tag{32}$$

for three-dimensions. Application of the Fourier transform to classical general schemes gives the same numerical wave numbers for both two and three-dimensions:

$$(k_1\Delta x)_c^* = \sum_{n=-N}^{N} a_n e^{nlk_1\Delta x}, \tag{33}$$

Table 1
Coefficients of various explicit centered finite difference schemes

Scheme	$a_1 = -a_{-1}$	$a_2 = -a_{-2}$	$a_3 = -a_{-3}$
Second order centered	1/2	0	0
Fourth order centered	2/3	−1/12	0
Sixth order centered	3/4	−3/20	1/60
Fourth order DRP [22]	0.7708824	−0.1667059	0.0208431

$$(k_2\Delta y)_c^* = \sum_{n=-N}^{N} a_n e^{nIk_2\Delta y}, \tag{34}$$

$$(k_3\Delta z)_c^* = \sum_{n=-N}^{N} a_n e^{nIk_3\Delta z}, \tag{35}$$

where $I = \sqrt{-1}$. For the optimized general schemes the numerical wave numbers for three-dimensions are different from those corresponding to two-dimensions. For two-dimensions, the numerical wave numbers are

$$(k_1\Delta x)_{\text{opt}}^* = \frac{2}{(1+\beta)} \sum_{n=-N}^{N} a_n \left\{ e^{nIk_1\Delta x} + \frac{\beta}{2}\left[e^{nI(k_1\Delta x + k_2\Delta y)} + e^{nI(k_1\Delta x - k_2\Delta y)}\right]\right\}, \tag{36}$$

$$(k_2\Delta y)_{\text{opt}}^* = \frac{2}{(1+\beta)} \sum_{n=-N}^{N} a_n \left\{ e^{nIk_2\Delta y} + \frac{\beta}{2}\left[e^{nI(k_1\Delta x + k_2\Delta y)} - e^{nI(k_1\Delta x - k_2\Delta y)}\right]\right\}, \tag{37}$$

and for three-dimensions they are:

$$\begin{aligned}(k_1\Delta x)_{\text{opt}}^* = \frac{2}{(1+2\beta)} \sum_{n=-N}^{N} a_n \Bigg\{ & e^{nIk_1\Delta x} + \frac{\beta}{2}\Big[e^{nI(k_1\Delta x + k_2\Delta y + k_3\Delta z)} + e^{nI(-k_1\Delta x + k_2\Delta y + k_3\Delta z)} \\ & + e^{nI(-k_1\Delta x - k_2\Delta y + k_3\Delta z)} + e^{nI(-k_1\Delta x + k_2\Delta y - k_3\Delta z)}\Big]\Bigg\},\end{aligned} \tag{38}$$

$$\begin{aligned}(k_2\Delta y)_{\text{opt}}^* = \frac{2}{(1+2\beta)} \sum_{n=-N}^{N} a_n \Bigg\{ & e^{nIk_2\Delta y} + \frac{\beta}{2}\Big[e^{nI(k_1\Delta x + k_2\Delta y + k_3\Delta z)} \\ & + e^{nI(k_1\Delta x - k_2\Delta y - k_3\Delta z)} + e^{nI(-k_1\Delta x - k_2\Delta y + k_3\Delta z)} + e^{nI(k_1\Delta x - k_2\Delta y + k_3\Delta z)}\Big]\Bigg\},\end{aligned} \tag{39}$$

$$\begin{aligned}(k_1\Delta x)_{\text{opt}}^* = \frac{2}{(1+2\beta)} \sum_{n=-N}^{N} a_n \Bigg\{ & e^{nIk_1\Delta x} + \frac{\beta}{2}\Big[e^{nI(-k_1\Delta x + k_2\Delta y - k_3\Delta z)} + e^{nI(-k_1\Delta x + k_2\Delta y + k_3\Delta z)} \\ & + e^{nI(k_1\Delta x - k_2\Delta y - k_3\Delta z)} + e^{nI(k_1\Delta x + k_2\Delta y - k_3\Delta z)}\Big]\Bigg\}.\end{aligned} \tag{40}$$

Eq. (33) representing the numerical wave number for the classical x derivative stencil is dependent only on $k_1\Delta x$ variable which corresponds to the x-direction. As seen, for example, in Eq. (36) the numerical wave number of the optimized stencil approximating the x derivative is dependent on both $k_1\Delta x$ and $k_2\,\Delta y$ variables that correspond to the x and y directions, respectively. Therefore, multidimensional optimizations by varying ICF are possible.

As an example, the fourth order optimized schemes in two-dimensions and the corresponding numerical wave numbers and numerical dispersion relation are

$$\begin{aligned}\left(\frac{\partial u}{\partial x}\right)_{i,j} = \frac{1}{12\Delta x(1+\beta)} \Bigg[& u_{i-2,j} - 8u_{i-1,j} + 8u_{i+1,j} - u_{i+2,j} + \frac{\beta}{2}(u_{i-2,j-2} - 8u_{i-1,j-1} + 8u_{i+1,j+1} \\ & - u_{i+2,j+2} - u_{i+2,j-2} + 8u_{i+1,j-1} - 8u_{i-1,j+1} + u_{i-2,j+2})\Bigg],\end{aligned} \tag{41}$$

$$\begin{aligned}\left(\frac{\partial u}{\partial y}\right)_{i,j} = \frac{1}{12\Delta y(1+\beta)} \Bigg[& u_{i,j-2} - 8u_{i,j-1} + 8u_{i,j+1} - u_{i,j+2} + \frac{\beta}{2}(u_{i-2,j-2} - 8u_{i-1,j-1} + 8u_{i+1,j+1} \\ & - u_{i+2,j+2} + u_{i+2,j-2} - 8u_{i+1,j-1} + 8u_{i-1,j+1} - u_{i-2,j+2})\Bigg],\end{aligned} \tag{42}$$

$$\begin{aligned}(k_1\Delta x)_{\text{opt}}^* = \frac{1}{6(1+\beta)} \Bigg\{ & 8\sin(k_1\Delta x) - \sin(2k_1\Delta x) + \frac{\beta}{2}[8\sin(k_1\Delta x + k_2\Delta y) - \sin(2k_1\Delta x + 2k_2\Delta y) \\ & + 8\sin(k_1\Delta x - k_2\Delta y) - \sin(2k_1\Delta x - 2k_2\Delta y)]\Bigg\},\end{aligned} \tag{43}$$

$$(k_2\Delta y)^*_{\text{opt}} = \frac{1}{6(1+\beta)}\left\{8\sin(k_2\Delta y) - \sin(2k_2\Delta y) + \frac{\beta}{2}[8\sin(k_1\Delta x + k_2\Delta y) - \sin(2k_1\Delta x + 2k_2\Delta y) - 8\sin(k_1\Delta x - k_2\Delta y) + \sin(2k_1\Delta x - 2k_2\Delta y)]\right\}, \tag{44}$$

$$\omega^2 - [(k_1\Delta x)^{*2}_{\text{opt}} + (k_2\Delta y)^{*2}_{\text{opt}}] = 0. \tag{45}$$

The time integration is supposed to be again free of numerical dissipation and dispersion. The ICF for higher-order optimized schemes is smaller compared to that of the optimized second order scheme. This is explained by the fact that the higher-order schemes have smaller isotropy error compared to lower-order schemes. For the fourth order centered optimized scheme ICF is approximately 0.26, and for the sixth order centered optimized scheme it is approximately 0.16.

3.4. Boundary stencils

Optimized boundary stencils are derived in this section for two-dimensions. The generalization to three-dimensions is straightforward. For a boundary point both x- and y derivative must be differently discretized because the interior stencils are not applicable for the direction along the boundaries. If the boundary is perpendicular to x-direction (see Fig. 5) the second order optimized stencils for x and y derivatives are derived in the same manner, using the weighted averaging. The x and y derivatives are given by:

$$\left(\frac{\partial u}{\partial x}\right)_{i,j} = \frac{1}{2\Delta x(1+\beta)}\left[-3u_{i,j} + 4u_{i+1,j} - u_{i+2,j} + \frac{\beta}{2}(-3u_{i,j} + 4u_{i+1,j+1} - u_{i+2,j+2} - 3u_{i,j} + 4u_{i+1,j-1} - u_{i+2,j-2})\right], \tag{46}$$

$$\left(\frac{\partial u}{\partial y}\right)_{i,j} = \frac{1}{2\Delta y(1+\beta)}\left[u_{i,j+1} - u_{i,j-1} + \frac{\beta}{2}(-3u_{i,j} + 4u_{i+1,j+1} - u_{i+2,j+2} + 3u_{i,j} - 4u_{i+1,j-1} + u_{i+2,j-2})\right]. \tag{47}$$

The numerical wave numbers are

$$(k_1\Delta x)^*_{\text{opt}} = \frac{1}{2(1+\beta)}\left\{4\sin(k_1\Delta x) - \sin(2k_1\Delta x) + \frac{\beta}{2}[4\sin(k_1\Delta x + k_2\Delta y) - \sin(2k_1\Delta x + 2k_2\Delta y) + 4\sin(k_1\Delta x - k_2\Delta y) - \sin(2k_1\Delta x - 2k_2\Delta y)]\right\}$$
$$+\frac{I}{2(1+\beta)}\left\{3 - 4\cos(k_1\Delta x) + \cos(2k_1\Delta x) + \frac{\beta}{2}[6 - 4\cos(k_1\Delta x + k_2\Delta y) + \cos(2k_1\Delta x + 2k_2\Delta y) - 4\cos(k_1\Delta x - k_2\Delta y) + \cos(2k_1\Delta x - 2k_2\Delta y)]\right\}, \tag{48}$$

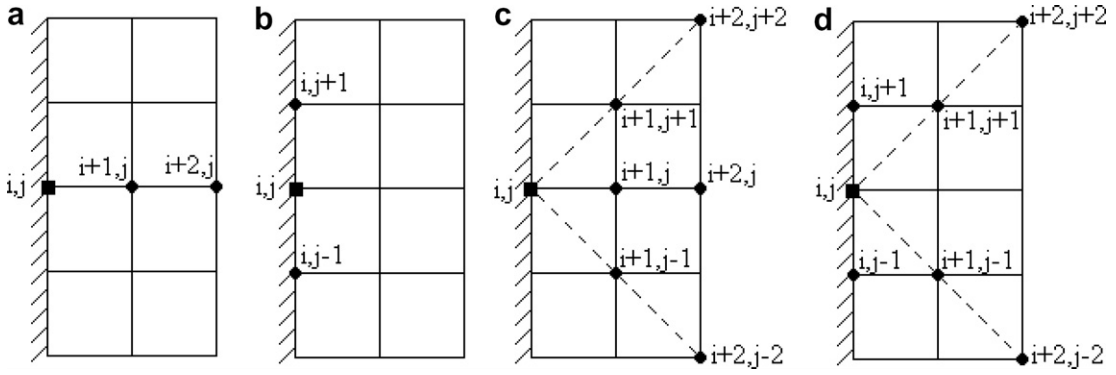

Fig. 5. Points used by boundary classical second order schemes for the (a) x derivative; (b) y derivative and by the boundary optimized second order schemes for the; (c) x derivative and (d) y derivative.

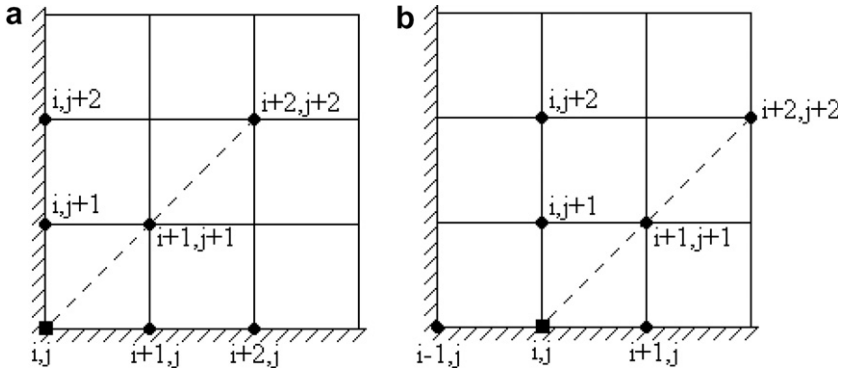

Fig. 6. Points used by optimized second order schemes (a) in corner and (b) near the corner.

$$
\begin{aligned}
(k_2\Delta y)^*_{\text{opt}} = {} & \frac{1}{2(1+\beta)}\left\{2\sin(k_2\Delta y)+\frac{\beta}{2}[4\sin(k_1\Delta x+k_2\Delta y)-\sin(2k_1\Delta x+2k_2\Delta y)\right. \\
& \left.-4\sin(k_1\Delta x-k_2\Delta y)+\sin(2k_1\Delta x-2k_2\Delta y)]\right\} \\
& +\frac{I}{2(1+\beta)}\left\{\frac{\beta}{2}[-4\cos(k_1\Delta x+k_2\Delta y)+\cos(2k_1\Delta x+2k_2\Delta y)\right. \\
& \left.+4\cos(k_1\Delta x-k_2\Delta y)-\cos(2k_1\Delta x-2k_2\Delta y)]\right\}. \qquad (49)
\end{aligned}
$$

The numerical wave numbers for boundary points in Eqs. (48) and (49) have both real and imaginary parts corresponding to dispersion and dissipation, respectively. ICF can be found taking into account either the real, or the imaginary part of the numerical dispersion relation, depending on whether the optimization is performed in terms of dispersion or dissipation, respectively. In this work, the ICF for the boundary stencils is determined by requiring that the dispersion be the same in both x and $x = y$ directions as for the interior schemes (this will be treated in Section 3.5). The optimization of the boundary stencils in terms of lowering the dissipation will be considered in a future paper. The points used by the classical and optimized boundary schemes are shown in Fig. 5.

Special care must be taken at the corners. The points used by the optimized second order schemes in the corner and near the corner are sketched in Fig. 6, and the optimized second order schemes for a corner point are given by Eqs. (50) and (51) and near the corner by Eqs. (52) and (53).

$$\left(\frac{\partial u}{\partial x}\right)_{i,j}=\frac{1}{2\Delta x(1+\beta)}\left[\left(1+\frac{\beta}{2}\right)(-3u_{i,j}+4u_{i+1,j}-u_{i+2,j})+\frac{\beta}{2}(4u_{i+1,j+1}-u_{i+2,j+2}-4u_{i,j+1}+u_{i,j+2})\right], \qquad (50)$$

$$\left(\frac{\partial u}{\partial y}\right)_{i,j}=\frac{1}{2\Delta y(1+\beta)}\left[\left(1+\frac{\beta}{2}\right)(-3u_{i,j}+4u_{i,j+1}-u_{i,j+2})+\frac{\beta}{2}(-4u_{i+1,j+1}+u_{i+2,j+2}+4u_{i+1,j}-u_{i+2,j})\right] \qquad (51)$$

for a corner point, and

$$\left(\frac{\partial u}{\partial x}\right)_{i,j}=\frac{1}{2\Delta x(1+\beta)}\left[\left(1+\frac{\beta}{2}\right)(u_{i+1,j}-u_{i-1,j})+\frac{\beta}{2}(-4u_{i+1,j+1}+u_{i+2,j+2}+4u_{i,j+1}-u_{i,j+2})\right], \qquad (52)$$

$$\left(\frac{\partial u}{\partial y}\right)_{i,j}=\frac{1}{2\Delta y(1+\beta)}\left[\left(1+\frac{\beta}{2}\right)(-3u_{i,j}+4u_{i+1,j}-u_{i+2,j})+\frac{\beta}{2}(-3u_{i,j}+4u_{i+1,j+1}-u_{i+2,j+2}+u_{i-1,j}-u_{i+1,j})\right] \qquad (53)$$

near the corner. For higher-order stencils more points near the corner must be taken into account in different manner (every such point will require a different stencil).

In the Appendix, it is shown that the order of accuracy of the optimized schemes is the same as that of the classical schemes for second, fourth, and sixth order centered schemes. The advantage is in terms of isotropy error which can be considerably lowered by varying the ICF. The value of ICF is calculated in the next subsection.

3.5. ICF calculation

ICF is found by minimizing the integrated error between the phase or group velocities on the x and $x = y$ directions in two-dimensions or the x and $x = y = z$ directions in three direction. For the sake of simplicity the two-dimensional case is considered. Two curves in the wavenumber–frequency space are considered: one of them is the intersection between the numerical dispersion relation surface (Fig. 3(b)) and $k_2 = 0$ plane, Eq. (54), and the other is the intersection between the numerical dispersion relation surface and the $k_1 = k_2$ plane, Eq. (55):

$$\begin{cases} \omega^2 - \left[(k_1\Delta x)^{*2}_{\text{opt}} + (k_2\Delta y)^{*2}_{\text{opt}}\right] = 0 \\ k_2 = 0 \end{cases}, \tag{54}$$

$$\begin{cases} \omega^2 - \left[(k_1\Delta x)^{*2}_{\text{opt}} + (k_2\Delta y)^{*2}_{\text{opt}}\right] = 0 \\ k_1 = k_2 \end{cases}. \tag{55}$$

These two curves are superposed in the $(k\Delta x, \omega)$ plane, where

$$k\Delta x = [(k_1\Delta x)^2 + (k_2\Delta y)^2]^{\frac{1}{2}} \tag{56}$$

Suppose that the equations of the two curves in $(k\Delta x, \omega)$ plane are

$$\omega_1 = \omega_1(k\Delta x, \beta), \tag{57}$$

$$\omega_2 = \omega_2(k\Delta x, \beta). \tag{58}$$

The integrated error between the phase velocities is then calculated on a specified interval (0–η here):

$$C(\beta) = \int_0^\eta |c_1(k\Delta x, \beta) - c_2(k\Delta x, \beta)|^2 d(k\Delta x), \tag{59}$$

where

$$c_1(k\Delta x, \beta) = \frac{\omega_1(k\Delta x, \beta)}{k\Delta x} \quad \text{and} \quad c_2(k\Delta x, \beta) = \frac{\omega_2(k\Delta x, \beta)}{k\Delta x} \tag{60}$$

are the phase velocities corresponding to Eqs. (54) and (55). The value of η is dependent on the scheme to be optimized (for example, $\eta = 1$ for the second order centered scheme). The optimization can also be performed using the integrated error between the group velocities by

$$G(\beta) = \int_0^\eta |g_1(k\Delta x, \beta) - g_2(k\Delta x, \beta)|^2 \, \mathrm{d}(k\Delta x), \tag{61}$$

where

$$g_1(k\Delta x, \beta) = \frac{\partial\omega_1(k\Delta x, \beta)}{\partial(k\Delta x)} \quad \text{and} \quad g_2(k\Delta x, \beta) = \frac{\partial\omega_2(k\Delta x, \beta)}{\partial(k\Delta x)} \tag{62}$$

are the group velocities corresponding to Eqs. (54) and (55). The minimization is done by equalizing the first derivative of $C(\beta)$ or $G(\beta)$ with zero:

$$\frac{\mathrm{d}C(\beta)}{\mathrm{d}\beta} = 0 \quad \text{or} \quad \frac{\mathrm{d}G(\beta)}{\mathrm{d}\beta} = 0 \tag{63}$$

which gives the value of ICF. For the second order centered schemes $\beta \cong 0.53$, for the fourth order centered schemes $\beta \cong 0.282$, and for the sixth order centered schemes $\beta \cong 0.152$. In Figs. 7–9 polar diagrams of normal-

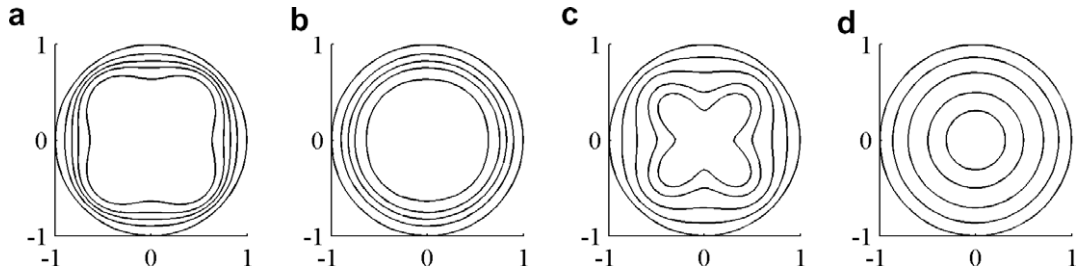

Fig. 7. Polar diagram of normalized phase velocities (a and b) and group velocities (c and d) as a function of points per wavelength and the direction of propagation: (a) and (c) using second order classical schemes; (b) and (d) using second order optimized schemes. Starting from interior the curves correspond to 4, 5, 6, 8 and ∞ points per wavelength for (a) and (b), and 5, 6, 8, 12 and ∞ points per wavelength for (c) and (d).

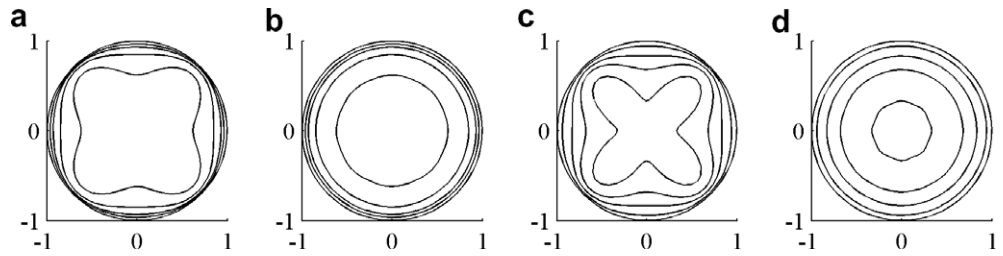

Fig. 8. Polar diagram of normalized phase velocities (a and b) and group velocities (c and d) as a function of points per wavelength and the direction of propagation: (a) and (c) using fourth order classical schemes; (b) and (d) using fourth order optimized schemes. Starting from interior the curves correspond to 3, 4, 5, 6 and ∞ points per wavelength for (a) and (b), and 4, 5, 6, 8 and ∞ points per wavelength for (c) and (d).

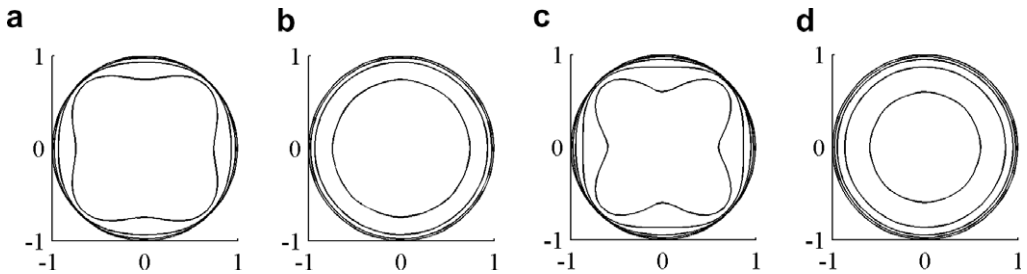

Fig. 9. Polar diagram of normalized phase velocities (a and b) and group velocities (c and d) as a function of points per wavelength and the direction of propagation: (a) and (c) using sixth order classical schemes; (b) and (d) using sixth order optimized schemes. Starting from interior the curves correspond to 3, 4, 5 and ∞ points per wavelength for (a) and (b), and 4, 5, 6, 7 and ∞ points per wavelength for (c) and (d).

ized phase or group velocities for different centered classical and optimized schemes are shown. The diagrams are plotted for different numbers of points per wavelength (ppw).

The idea can be easily extended to any explicit finite difference schemes of any order. For example, the high efficiency of dispersion-relation-preserving (DRP) scheme of Tam and Webb [22] in one-dimension can be extended to multidimensions: its high-resolution characteristics can be combined with a good isotropy. For the DRP scheme there is a particular value of the number of points per wavelength which makes the numerical dispersion relation to be the same as the exact dispersion relation. For a multidimensional problem, this is true only along the grid lines. By using the idea developed in this work, this can be achieved for any direction in the sense that the DRP characteristics are conserved for additional two directions (aligned at 45° with respect to the grid lines) and kept very accurate for any other direction (as Figs. 7–9 would show for some explicit schemes).

The extension to compact schemes may be obvious, but the effort of solving large sets of equations is too high. In case of a possible compact optimized scheme the matrix for the derivatives calculation in the grid points is no longer constructed along a grid line, but on the entire grid, probably. Also, it is envisioned that the matrices to be solved may have at least 7 diagonals (for the simplest case of fourth order accurate compact schemes).

4. Results

First a two-dimensional problem from First Computational Aeroacoustics Workshop [4] is considered. An acoustic wave at O(0, 0) point and an entropy wave at $P(67, 67)$ point are transported with the mean flow along the $x = y$ directions (Fig. 10). The linearized two-dimensional Euler equations on a uniform mean flow are considered:

$$\frac{\partial Q}{\partial t} + \frac{\partial E}{\partial x} + \frac{\partial F}{\partial y} = 0, \tag{64}$$

where

$$Q = \begin{bmatrix} \rho' \\ u' \\ v' \\ p' \end{bmatrix}, \quad E = \begin{bmatrix} M_x\rho' + u' \\ M_x u' + p' \\ M_x v' \\ M_x p' + u' \end{bmatrix}, \quad F = \begin{bmatrix} M_y\rho' + v' \\ M_y u' \\ M_y v' + p' \\ M_y p' + v' \end{bmatrix}. \tag{65}$$

M_x and M_y are constant mean flow Mach numbers in x and y directions, respectively. The computational domain embedded in free space is $-100 < x < 100$, $-100 < y < 100$, and x- and y-component of the Mach number are

$$M_x = M_y = 0.5\cos\left(\frac{\pi}{4}\right). \tag{66}$$

The initial conditions are Gaussian impulses:

$$p' = \mathrm{e}^{-(\ln 2)\left(\frac{x^2+y^2}{9}\right)}, \tag{67}$$

$$\rho' = \mathrm{e}^{-(\ln 2)\left(\frac{x^2+y^2}{9}\right)} + 0.1 \cdot \mathrm{e}^{-(\ln 2)\left(\frac{(x-67)^2+(y-67)^2}{25}\right)}, \tag{68}$$

$$u' = 0.04 \cdot (y - 67) \cdot \mathrm{e}^{-(\ln 2)\left(\frac{(x-67)^2+(y-67)^2}{25}\right)}, \tag{69}$$

$$v' = -0.04 \cdot (x - 67) \cdot \mathrm{e}^{-(\ln 2)\left(\frac{(x-67)^2+(y-67)^2}{25}\right)}. \tag{70}$$

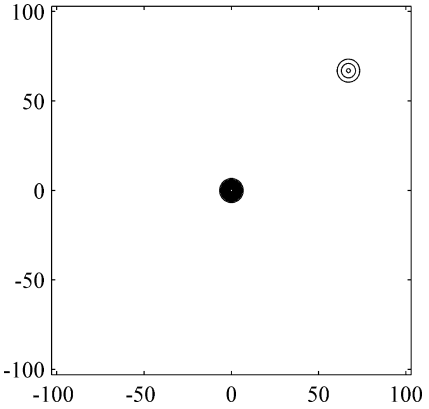

Fig. 10. Initial condition for the Computational Aeroacoustics Workshop problem.

The problem is solved using three types of optimized centered finite difference schemes (second, fourth, and sixth order). The domain was discretized using equally-spaced grid on x and y directions with $\Delta x = \Delta y = 0.5$ for second order schemes, $\Delta x = \Delta y = 0.75$ for fourth order schemes and $\Delta x = \Delta y = 1$ for sixth order schemes: Table 2 summarizes the number of points of the grids and the corresponding optimized stencils used. One, two or three rows of grid points were considered outside the boundary for the application of non-reflecting boundary conditions based on ghost points corresponding to second, fourth and sixth order schemes, respectively.

At the boundaries non-reflecting and inflow–outflow boundary conditions of Tam and Webb [22,23] are used. Filtering techniques of Kennedy and Carpenter [12] were included to annihilate the spurious waves. The constant coefficient explicit sixth order filter is used for the second order optimized schemes, explicit eighth order filter for the fourth order optimized schemes and 10th order filter for the sixth order optimized schemes. The influence of the classical filters over the optimized schemes is expected to be weak because filters are generally designed to act over the high wavenumber interval, whereas the optimization is performed mostly on the low wavenumber interval. Future work includes the optimization of the filters to include points from more than one direction. Low-Dissipation and -Dispersion 4–6 Runge–Kutta scheme of Hu et al. [11] is used for time integration. The time step was calculated by requiring the stability limit of the two-dimensional convection equation which is discretized using optimized centered schemes (details regarding the stability analysis for the optimized schemes will be provided in a future paper). Results for time equal to 80 are given in Figs. 11–13. The numerical results are compared to analytical results.

In addition, some numerical tests on the stationary fluid ($M_x = M_y = 0$) were made by modifying the first problem: acoustic wave is propagating from origin, and the entropy wave is neglected. The domain was extended to $-400 < x < 400$, $-400 < y < 400$, such that the wave can propagate for a longer time; the space step is $\Delta x = \Delta\ y = 0.5$. The front waves of the acoustic pressure on x, and $x = y$ directions are compared (Fig. 14). The second order optimized centered schemes and their corresponding classical schemes are compared this time in order to reveal the anisotropy correction. While Fig. 14(a) shows that the front waves computed using classical schemes do not coincide, in Fig. 14(b) for which optimized second order schemes were used the matching of the two front waves is obvious.

Table 2
Number of grid points used for different cases

Schemes	Number of grid points along x and y directions
Second order	400
Fourth order	300
Sixth order	200

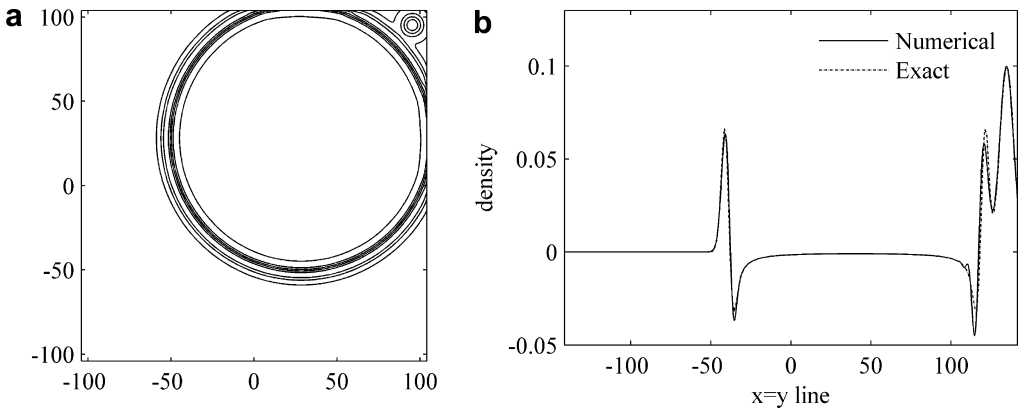

Fig. 11. (a) Density contours and (b) density distribution along the $x = y$-direction for the Computational Aeroacoustics Workshop problem using optimized second order schemes.

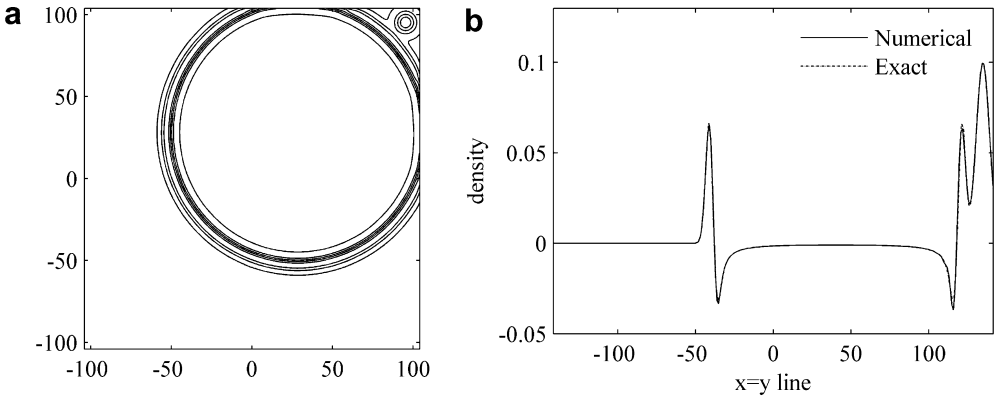

Fig. 12. (a) Density contours and (b) density distribution along the $x = y$-direction for the Computational Aeroacoustics Workshop problem using optimized fourth order schemes.

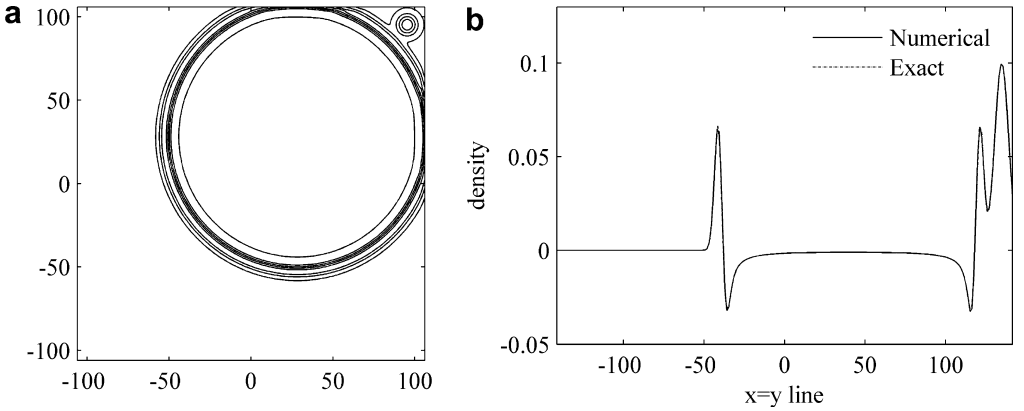

Fig. 13. (a) Density contours and (b) density distribution along the $x = y$-direction for the Computational Aeroacoustics Workshop problem using optimized sixth order schemes.

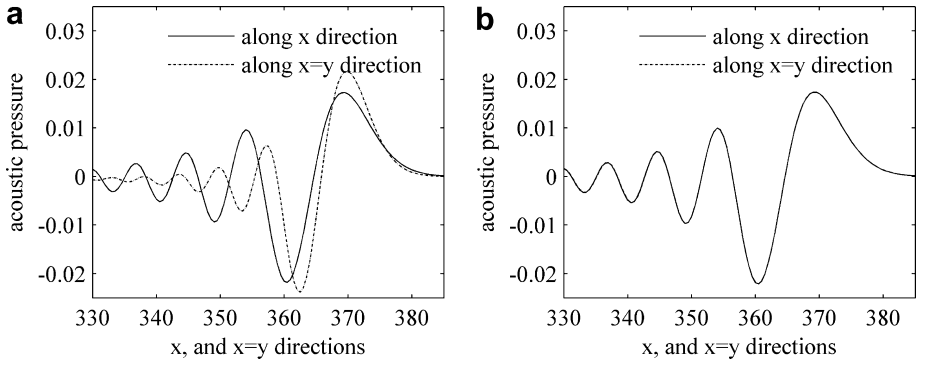

Fig. 14. Superposed front waves on the x, and $x = y$ directions using (a) classical and (b) optimized second order schemes.

The previous analysis is extended to a three-dimensional problem: spherical wave propagating from origin. The domain is a cube embedded in free space, $-50 < x < 50$, $-50 < y < 50$, $-50 < z < 50$, and the space step is $\Delta x = \Delta y = \Delta z = 0.5$. Non-reflecting boundary conditions of Tam and Webb [22,23] is used at the all boundaries as before. The same Low-Dissipation and -Dispersion 4–6 Runge–Kutta Scheme of Hu et al. [11] is used

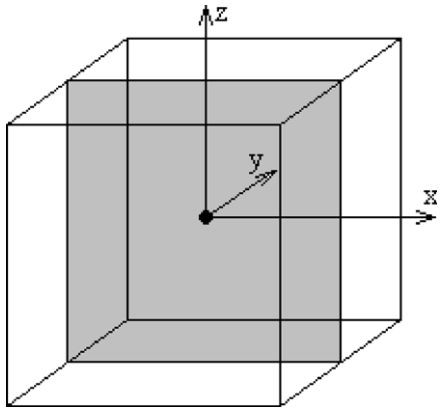

Fig. 15. The $y = 0$ plane section, where the pressure contours in Fig. 16 are plotted.

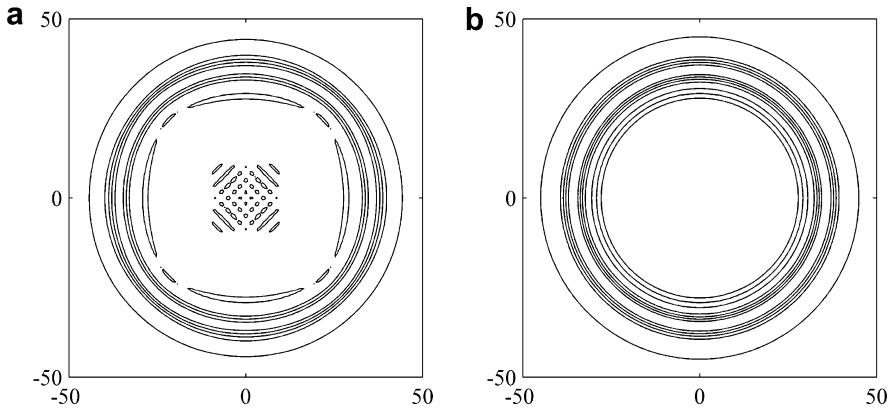

Fig. 16. Pressure contours in the plane section depicted in Fig. 15 using (a) classical and (b) optimized second order schemes.

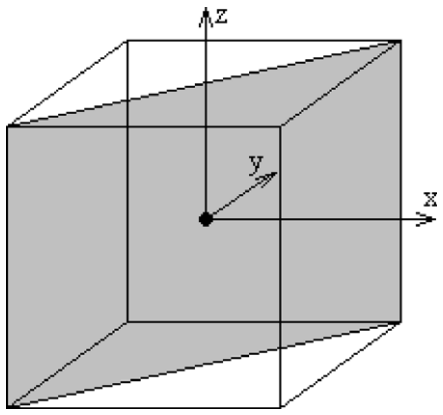

Fig. 17. The $x = y$ plane section where the pressure contours in Fig. 18 are plotted.

for time integration. Filtering technique [12] with constant coefficients and of 6th order was used to take care of spurious waves. The acoustic pressure contours in the $y = 0$ (Fig. 15) and $x = y$ (Fig. 17) planes determined using optimized second order schemes are compared to contours determined using classical schemes (Figs. 16 and 18). Also the front waves along the x and $x = y = z$ directions are superposed and compared for both using classical and optimized schemes (Fig. 19).

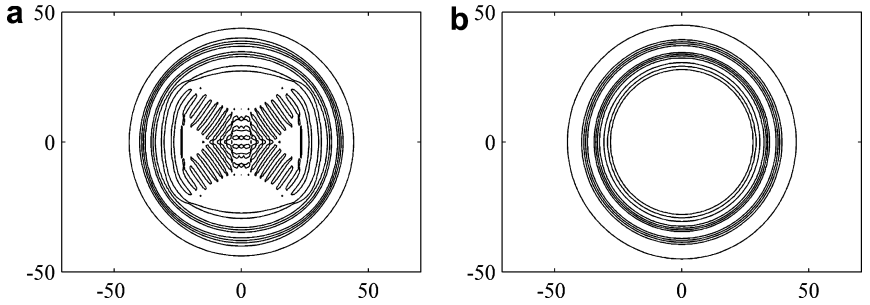

Fig. 18. Pressure contours on the plane section depicted in Fig. 17 using (a) classical and (b) optimized second order schemes.

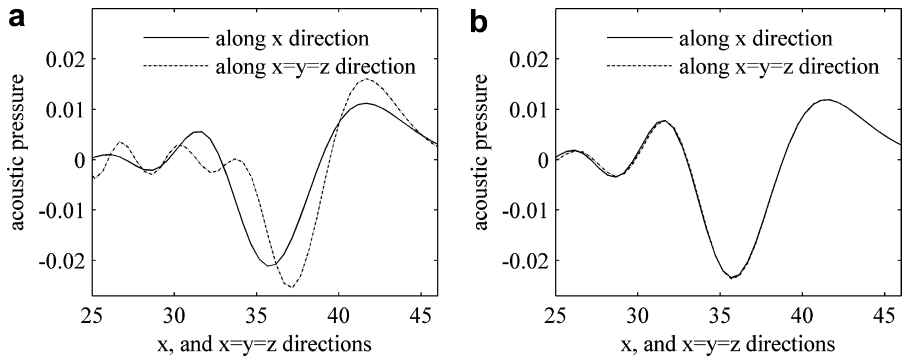

Fig. 19. Superposed front waves on the x, and $x = y = z$ directions using (a) classical and (b) optimized second order schemes.

Figs. 16 and 18 show that the optimized schemes correct the anisotropy, and also annihilate the spurious waves more effectively compared to using classical schemes.

The optimized schemes are suitable to generalized curvilinear transformation methods. To analyze the effect of the grid stretching, the previous two-dimensional wave propagation from origin is computed using second order classical and optimized centered schemes on the stretched grid. The grid is stretched along y-direction in the vicinity of $y = 0$ (center of the domain, Fig. 20). The relations defining the grid stretching are

$$F(\alpha_1, \alpha_2) = \frac{1}{2\alpha_2} \ln\left[\frac{1 + (e^{\alpha_2} - 1)\alpha_1}{1 + (e^{-\alpha_2} - 1)\alpha_1}\right], \tag{71}$$

$$y_j = L_y \cdot \alpha_1 \cdot \left\{1 + \frac{\sinh\left[\alpha_2\left(\frac{j-1}{N_y-1}\right) - F(\alpha_1, \alpha_2)\right]}{\sinh\left[\alpha_2\left(\frac{j-1}{N_y-1}\right)\right]}\right\}, \tag{72}$$

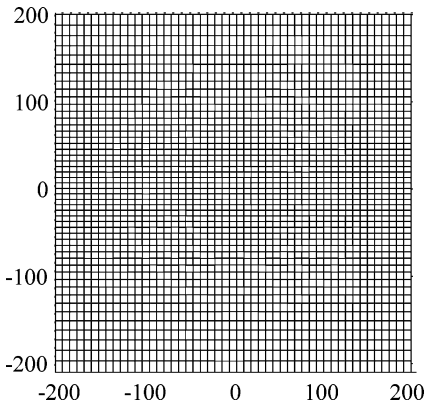

Fig. 20. Stretched grid for the last problem.

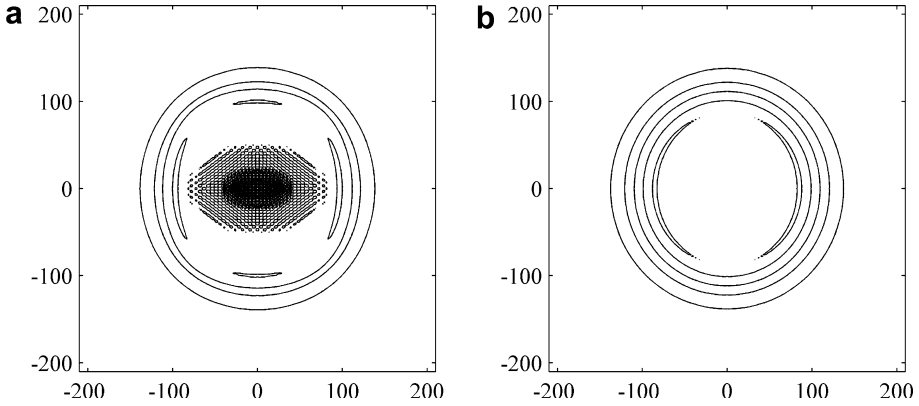

Fig. 21. Wave propagating from origin on the stretched grid (Fig. 20) using (a) classical second order schemes and (b) optimized second order schemes.

where α_1 and α_2 are the stretching parameters, j is the grid index along y-direction, L_y is the length of the domain along y-direction and N_y is the number of grid points along this direction. α_1 controls the position of stretching, and the value of 0.5 sets the minimum Δy in the middle of the domain ($y = 0$). α_2 is called stretching factor and controls the intensity of the stretching: $\alpha_2 = 1$ corresponds to a non-stretched grid, $\alpha_2 > 1$ decreases and $\alpha_2 < 1$ increases the grid spacing. The Linearized Euler Equations are transformed into generalized curvilinear form, and the actual domain defined in (x, y) coordinate is mapped into the computational domain with (ξ, η) coordinates. The equations are solved in the computational domain with the step size of $\Delta\xi = \Delta\eta = 1$.

To reveal the difference in spurious waves generated by the classical and optimized schemes, this time the solver does not use filtering techniques. Results for the second order classical and optimized schemes are given in Fig. 21. Generalized curvilinear transformation is used to solve the Linearized Euler Equations, and the derivatives for grid metrics calculation are discretized using optimized schemes. For the same stretching factor it was observed that, while the classical schemes produce spurious waves due to stretching (in other words the solver is going to blow up), the optimized schemes do not. In conclusion, the optimized schemes are more stable compared to the classical schemes when using curvilinear coordinates. This is also the case even if the stretching factor for the optimized schemes is increased (with approximately 20% from the stretching factor of the classical schemes) suggesting the fact that the optimized schemes are more effective for curvilinear transformation methods.

5. Concluding remarks

Anisotropy correction of multidimensional finite difference schemes was carried out for interior and boundary stencils. It was shown that the numerical derivation based on finite difference schemes in multidimensions using points along the grid lines may cause serious isotropy error, especially for lower-order accurate schemes. Therefore, there is a need for deriving difference schemes that use points from other directions. The optimized schemes incorporate a parameter called isotropy corrector factor (ICF) which can lower the isotropy error to a large extent. Based on Fourier analysis ICF was found and it was shown that, in terms of isotropy error, the optimized schemes are more effective compared to classical schemes. The optimized schemes are linear combinations of classical schemes, such that the order of accuracy is unchanged. Boundary optimized schemes were derived and possible problems were emphasized; for example, the application of the boundary conditions based on ghost points. For corner points the derivation of the optimized higher-order schemes can be arduous because every point in the corner and near the corner requires a different stencil.

Selected test problems were solved using both classical and optimized schemes, and the results were compared to each other or to analytical results. The anisotropy correction was successful for both two- and three-dimensional applications that involved wave propagation. It was shown that in case of the curvilinear

transformation the optimized schemes yield less spurious waves in comparison to classical schemes. This was even more convincing by the use of a larger stretching factor for the case of using optimized schemes. The large amplitude spurious waves produced by the classical schemes are due to the isotropy error resulting from the calculation of the grid metrics.

It was shown that the optimized schemes preserve the characteristics of the corresponding classical one-dimensional schemes for all spatial directions. This is an important result because one needs to control the errors in all directions for multidimensional problems.

A primary disadvantage is the boundary conditions implementation, especially those based on ghost points. Additionally, computation time increased with a factor of 1.075 to 1.3 depending on the schemes used or on the solver. The optimized schemes are restricted to generalized curvilinear transformation and to Cartesian grid methods with equal grid step in all spatial directions.

Appendix

In appendix, it is shown that the order of accuracy of the second-, fourth- and sixth order optimized centered schemes is the same as that of the corresponding classical schemes. The Taylor series expansions of the terms in the optimized schemes are skipped (they could easily be written), and only the coefficients and their summations are written. The grid is equally-spaced, and $\Delta x = \Delta y$.

The coefficients of the Taylor series expansions for the two-dimensional second order optimized scheme on the x-direction:

$$\frac{\partial^0 u}{\partial x^0} : \frac{1}{2\Delta x(1+\beta)}\left[u_{i,j} - u_{i,j} + \frac{\beta}{2}(u_{i,j} - u_{i,j} + u_{i,j} - u_{i,j})\right] = 0,$$
$$\frac{\partial u}{\partial x} : \frac{\Delta x}{2\Delta x(1+\beta)}\left[1 + 1 + \frac{\beta}{2}(1+1+1+1)\right] = \frac{2\Delta x(1+\beta)}{2\Delta x(1+\beta)} = 1,$$
$$\frac{\partial u}{\partial y} : \frac{\Delta y}{2\Delta y(1+\beta)}\left[0 + \frac{\beta}{2}(1-1-1+1)\right] = 0,$$
$$\frac{\partial^2 u}{\partial x^2} : \frac{\Delta x^2}{2\Delta x(1+\beta)}\left[\frac{1}{2!} - \frac{1}{2!} + \frac{\beta}{2}\frac{1}{2!}(1-1+1-1)\right] = 0,$$
$$\frac{\partial^2 u}{\partial x \partial y} : \frac{\Delta x \Delta y}{2\Delta x(1+\beta)}\left[0 + \frac{\beta}{2}\frac{1}{2!}(2-2-2+2)\right] = 0,$$
$$\frac{\partial^2 u}{\partial y^2} : \frac{\Delta y^2}{2\Delta x(1+\beta)}\left[0 + \frac{\beta}{2}\frac{1}{2!}(1-1+1-1)\right] = 0.$$

The coefficients of the Taylor series expansions for the two-dimensional fourth order optimized scheme on x-direction:

$$\frac{\partial^0 u}{\partial x^0} : \frac{1}{12\Delta x(1+\beta)}\left[1 - 8 + 8 - 1 + \frac{\beta}{2}(1 - 8 + 8 - 1 + 1 - 8 + 8 - 1)\right] = 0,$$
$$\frac{\partial u}{\partial x} : \frac{\Delta x}{12\Delta x(1+\beta)}\left[-2 + 8 + 8 - 2 + \frac{\beta}{2}(-2 + 8 + 8 - 2 - 2 + 8 + 8 - 2)\right] = \frac{12\Delta x(1+\beta)}{12\Delta x(1+\beta)} = 1,$$
$$\frac{\partial u}{\partial y} : \frac{\Delta y}{12\Delta y(1+\beta)}\left[0 + \frac{\beta}{2}(-2 + 8 + 8 - 2 + 2 - 8 - 8 + 2)\right] = 0,$$
$$\frac{\partial^2 u}{\partial x^2} : \frac{\Delta x^2}{12\Delta x(1+\beta)2!}\left[4 - 8 + 8 - 4 + \frac{\beta}{2}(4 - 8 + 8 - 4 + 4 - 8 + 8 - 4)\right] = 0,$$
$$\frac{\partial^2 u}{\partial x \partial y} : \frac{\Delta x \Delta y}{12\Delta x(1+\beta)2!}\left[0 + \frac{\beta}{2}(8 - 16 + 16 - 8 + 8 - 16 + 16 - 8)\right] = 0,$$

$$\frac{\partial^2 u}{\partial y^2}:\frac{\Delta y^2}{12\Delta x(1+\beta)2!}\left[0+\frac{\beta}{2}(4-8+8-4+4-8+8-4)\right]=0,$$
$$\frac{\partial^3 u}{\partial x^3}:\frac{\Delta x^3}{12\Delta x(1+\beta)3!}\left[-8+8+8-8+\frac{\beta}{2}(-8+8+8-8-8+8+8-8)\right]=0,$$
$$\frac{\partial^3 u}{\partial x^2\partial y}:\frac{\Delta x^2\Delta y}{12\Delta x(1+\beta)3!}\left[0+\frac{\beta}{2}(-24+24+24-24+24-24-24+24)\right]=0,$$
$$\frac{\partial^3 u}{\partial x\partial y^2}:\frac{\Delta x\Delta y^2}{12\Delta x(1+\beta)3!}\left[0+\frac{\beta}{2}(-24+24+24-24-24+24+24-24)\right]=0,$$
$$\frac{\partial^3 u}{\partial y^3}:\frac{\Delta y^3}{12\Delta x(1+\beta)3!}\left[0+\frac{\beta}{2}(-8+8+8-8+8-8-8+8)\right]=0,$$
$$\frac{\partial^4 u}{\partial x^4}:\frac{\Delta x^4}{12\Delta x(1+\beta)4!}\left[16-8+8-16+\frac{\beta}{2}(16-8+8-16+16-8+8-16)\right]=0,$$
$$\frac{\partial^4 u}{\partial x^3\partial y}:\frac{\Delta x^3\Delta y}{12\Delta x(1+\beta)4!}\left[0+\frac{\beta}{2}(64-32+32-64-64+32-32+64)\right]=0,$$
$$\frac{\partial^4 u}{\partial x^2\partial y^2}:\frac{\Delta x^2\Delta y^2}{12\Delta x(1+\beta)4!}\left[0+\frac{\beta}{2}(96-48+48-96+96-48+48-96)\right]=0,$$
$$\frac{\partial^4 u}{\partial x\partial y^3}:\frac{\Delta x\Delta y^3}{12\Delta x(1+\beta)4!}\left[0+\frac{\beta}{2}(64-32+32-64-64+32-32+64)\right]=0,$$
$$\frac{\partial^4 u}{\partial y^4}:\frac{\Delta y^4}{12\Delta x(1+\beta)4!}\left[0+\frac{\beta}{2}(16-8+8-16+16-8+8-16)\right]=0.$$

The coefficients of the Taylor series expansions for the two-dimensional sixth order optimized scheme on the x-direction:

$$\frac{\partial^0 u}{\partial x^0}:\frac{u_{i,j}}{60\Delta x(1+\beta)}\left[1-9+45-45+9-1+\frac{\beta}{2}(1-9+45-45+9-1+1-9+45-45+9-1)\right]=0,$$
$$\frac{\partial u}{\partial x}:\frac{\Delta x}{60\Delta x(1+\beta)}\left[3-18+45+45-18+3+\frac{\beta}{2}(3-18+45+45-18+3+3-18+45+45-18+3)\right]$$
$$=\frac{60\Delta x(1+\beta)}{60\Delta x(1+\beta)}=1,$$
$$\frac{\partial u}{\partial y}:\frac{\Delta y}{60\Delta y(1+\beta)}\left[0+\frac{\beta}{2}(3-18+45+45-18+3-3+18-45-45+18-3)\right]=0,$$
$$\frac{\partial^2 u}{\partial x^2}:\frac{\Delta x^2}{60\Delta x(1+\beta)2!}\left[9-36+45-45+36-9+\frac{\beta}{2}(9-36+45\right.$$
$$\left.-45+36-9+9-36+45-45+36-9)\right]=0,$$
$$\frac{\partial^2 u}{\partial x\partial y}:\frac{\Delta x\Delta y}{60\Delta x(1+\beta)2!}\left[0+\frac{\beta}{2}(18-72+90-90+72-18+18-72+90-90+72-18)\right]=0,$$
$$\frac{\partial^2 u}{\partial y^2}:\frac{\Delta y^2}{60\Delta x(1+\beta)2!}\left[0+\frac{\beta}{2}(9-36+45-45+36-9+9-36+45\right.$$
$$\left.-45+36-9)\right]=0,$$
$$\frac{\partial^3 u}{\partial x^3}:\frac{\Delta x^3}{60\Delta x(1+\beta)3!}\left[27-72+45+45-72+27+\frac{\beta}{2}(27-72+45+45-72+27+27-72+45\right.$$
$$\left.+45-72+27)\right]=0,$$

$$\frac{\partial^3 u}{\partial x^2 \partial y}:\frac{\Delta x^2 \Delta y}{60\Delta x(1+\beta)3!}\left[0+\frac{\beta}{2}(81-216+135+135-216+81-81+216-135-135+216-81)\right]=0,$$

$$\frac{\partial^3 u}{\partial x \partial y^2}:\frac{\Delta x \Delta y^2}{60\Delta x(1+\beta)3!}\left[0+\frac{\beta}{2}(81-216+135+135-216+81+81-216+135+135-216+81)\right]=0,$$

$$\frac{\partial^3 u}{\partial y^3}:\frac{\Delta y^3}{60\Delta x(1+\beta)3!}\left[0+\frac{\beta}{2}(27-72+45-45+72-27-27+72-45+45-72+27)\right]=0,$$

$$\frac{\partial^4 u}{\partial x^4}:\frac{\Delta x^4}{60\Delta x(1+\beta)4!}\left[81-144+45-45-144+81+\frac{\beta}{2}(81-144+45-45-144+81+81 -144+45-45-144+81)\right]=0,$$

$$\frac{\partial^4 u}{\partial x^3 \partial y}:\frac{\Delta x^3 \Delta y}{60\Delta x(1+\beta)4!} \times\left[0+\frac{\beta}{2}(324-576+180-180+576-324+324-576+180-180+576-324)\right]=0,$$

$$\frac{\partial^4 u}{\partial x^2 \partial y^2}:\frac{\Delta x^2 \Delta y^2}{60\Delta x(1+\beta)4!} \times\left[0+\frac{\beta}{2}(486-864+270-270+864-486+486-864+270-270+864-486)\right]=0,$$

$$\frac{\partial^4 u}{\partial x \partial y^3}:\frac{\Delta x \Delta y^3}{60\Delta x(1+\beta)4!} \times\left[0+\frac{\beta}{2}(324-576+180-180+576-324-324+576-180+180-576+324)\right]=0,$$

$$\frac{\partial^4 u}{\partial y^4}:\frac{\Delta x^4}{60\Delta x(1+\beta)4!}\left[0+\frac{\beta}{2}(81-144+45-45-144+81+81-144+45-45-144+81)\right]=0,$$

$$\frac{\partial^5 u}{\partial x^5}:\frac{\Delta x^5}{60\Delta x(1+\beta)5!}\left[243-288+45-45+288-243+\frac{\beta}{2}(243-288+45-45+288-243-243 +288-45+45-288+243)\right]=0,$$

$$\frac{\partial^5 u}{\partial x^4 \partial y}:\frac{\Delta x^4 \Delta y}{60\Delta x(1+\beta)5!}\left[0+\frac{\beta}{2}(1215-1440+225+225-1440+1215-1215+1440-225-225 +1440-1215)\right]=0,$$

$$\frac{\partial^5 u}{\partial x^2 \partial y^3}:\frac{\Delta x^2 \Delta y^3}{60\Delta x(1+\beta)5!} \times\left[0+\frac{\beta}{2}(2430-2880+450-450+2880-2430+2430-2880+450-450+2880-2430)\right]=0,$$

$$\frac{\partial^5 u}{\partial x^3 \partial y^2}:\frac{\Delta x^3 \Delta y^2}{60\Delta x(1+\beta)5!} \times\left[0+\frac{\beta}{2}(2430-2880+450-450+2880-2430-2430+2880-450+450-2880+2430)\right]=0,$$

$$\frac{\partial^5 u}{\partial x \partial y^4}:\frac{\Delta x \Delta y^4}{60\Delta x(1+\beta)5!} \times\left[0+\frac{\beta}{2}(1215-1440+225+225-1440+1215+1215-1440+225+225-1440+1215)\right]=0,$$

$$\frac{\partial^5 u}{\partial y^5}:\frac{\Delta y^5}{60\Delta x(1+\beta)5!}\left[0+\frac{\beta}{2}(243-288+45-45+288-243-243+288-45+45-288+243)\right]=0,$$

$$\frac{\partial^6 u}{\partial x^6}:\frac{\Delta x^6}{60\Delta x(1+\beta)6!}\left[729-576+45-45+576-729+\frac{\beta}{2}(729-576+45-45+576-729+729\right.$$
$$\left.-576+45-45+576-729)\right]=0,$$
$$\frac{\partial^6 u}{\partial x^5\partial y}:\frac{\Delta x^5\Delta y}{60\Delta x(1+\beta)6!}\left[0+\frac{\beta}{2}(4374-3456+270-270+3456-4374-4374+3456\right.$$
$$\left.-225+225-3456+4374)\right]=0,$$
$$\frac{\partial^6 u}{\partial x^2\partial y^4}:\frac{\Delta x^2\Delta y^4}{60\Delta x(1+\beta)6!}\left[0+\frac{\beta}{2}(10935-8640+675-675+8640-10935+10935-8640+675\right.$$
$$\left.-675+8640-10935)\right]=0,$$
$$\frac{\partial^6 u}{\partial x^3\partial y^3}:\frac{\Delta x^3\Delta y^3}{60\Delta x(1+\beta)6!}\left[0+\frac{\beta}{2}(14580-11520+900-900+11520-14580-14580+11520-900\right.$$
$$\left.+900-11520+14580)\right]=0,$$
$$\frac{\partial^6 u}{\partial x^4\partial y^2}:\frac{\Delta x^4\Delta y^2}{60\Delta x(1+\beta)6!}\left[0+\frac{\beta}{2}(10935-8640+675-675+8640-10935+10935-8640+675\right.$$
$$\left.-675+8640-10935)\right]=0,$$
$$\frac{\partial^6 u}{\partial x\partial y^5}:\frac{\Delta x\Delta y^5}{60\Delta x(1+\beta)6!}\left[0+\frac{\beta}{2}(4374-3456+270-270+3456-4374-4374+3456-225\right.$$
$$\left.+225-3456+4374)\right]=0,$$
$$\frac{\partial^6 u}{\partial y^6}:\frac{\Delta y^6}{60\Delta x(1+\beta)6!}\left[729-576+45-45+576-729+\frac{\beta}{2}(729-576+45-45+576-729+729-576\right.$$
$$\left.+45-45+576-729)\right]=0.$$

The coefficients of the Taylor series expansions for the three-dimensional second order optimized scheme on the x-direction:

$$\frac{\partial^0 u}{\partial x^0}:\frac{1}{2\Delta x(1+2\beta)}\left[u_{i,j,k}-u_{i,j,k}+\frac{\beta}{2}(u_{i,j,k}-u_{i,j,k}+u_{i,j,k}-u_{i,j,k})\right]=0,$$
$$\frac{\partial u}{\partial x}:\frac{\Delta x}{2\Delta x(1+2\beta)}\left[1+1+\frac{\beta}{2}(1+1+1+1+1+1+1+1)\right]=\frac{2\Delta x(1+2\beta)}{2\Delta x(1+2\beta)}=1,$$
$$\frac{\partial u}{\partial y}:\frac{\Delta y}{2\Delta y(1+2\beta)}\left[0+\frac{\beta}{2}(1-1-1+1+1-1-1+1)\right]=0,$$
$$\frac{\partial u}{\partial z}:\frac{\Delta z}{2\Delta z(1+2\beta)}\left[0+\frac{\beta}{2}(1-1+1-1-1+1-1+1)\right]=0,$$
$$\frac{\partial^2 u}{\partial x^2}:\frac{\Delta x^2}{2\Delta x(1+2\beta)}\left[\frac{1}{2!}-\frac{1}{2!}+\frac{\beta}{2}\frac{1}{2!}(1-1+1-1+1-1+1-1)\right]=0,$$
$$\frac{\partial^2 u}{\partial y^2}:\frac{\Delta y^2}{2\Delta y(1+2\beta)}\left[0+\frac{\beta}{2}\frac{1}{2!}(1-1+1-1+1-1+1-1)\right]=0,$$

$$\frac{\partial^2 u}{\partial z^2} : \frac{\Delta z^2}{2\Delta z(1+2\beta)}\left[0+\frac{\beta}{2}\frac{1}{2!}(1-1+1-1+1-1+1-1)\right]=0,$$
$$\frac{\partial^2 u}{\partial x\partial y} : \frac{\Delta x\Delta y}{2\Delta x(1+2\beta)}\left[0+\frac{\beta}{2}\frac{1}{2!}(2+2-2-2+2+2-2-2)\right]=0,$$
$$\frac{\partial^2 u}{\partial x\partial z} : \frac{\Delta x\Delta z}{2\Delta x(1+2\beta)}\left[0+\frac{\beta}{2}\frac{1}{2!}(2+2+2+2-2-2-2-2)\right]=0,$$
$$\frac{\partial^2 u}{\partial y\partial z} : \frac{\Delta y\Delta z}{2\Delta x(1+2\beta)}\left[0+\frac{\beta}{2}\frac{1}{2!}(2+2-2-2-2-2+2+2)\right]=0.$$

Plugging the rest of the non-zero Taylor series terms into the schemes, it can be concluded that the order of accuracy of the optimized schemes is as expected. For example, the truncation error for the two-dimensional second order optimized scheme is

$$\varepsilon=\frac{(\Delta x)^2}{3}\frac{\partial^3 u}{\partial x^3}+\frac{2}{3}\left((\Delta x)^2\frac{\partial^3 u}{\partial x^3}+3(\Delta x)(\Delta y)\frac{\partial^3 u}{\partial x^2\partial y}+3(\Delta y)^2\frac{\partial^3 u}{\partial x\partial y^2}+\frac{(\Delta y)^3}{\Delta x}\frac{\partial^3 u}{\partial y^3}\right)+\ldots$$

and it is the order of $(\Delta x)^2$ as long as the grid is equally-spaced.

References

[1] G. Ashcroft, X. Zhang, Optimized prefactored compact schemes, J. Comput. Phys. 190 (2003) 459–477.
[2] C. Bogey, C. Bailly, A family of low dispersive and low dissipative explicit schemes for flow and noise computation, J. Comput. Phys. 194 (2004) 194–214.
[3] De A.K. Eswaran, Analysis of a new high resolution upwind compact scheme, J. Comput. Phys. 218 (2006) 398–416.
[4] J.C. Hardin, J.R. Ristorcelli, C.K.W. Tam, ICASE/LaRC Workshop on benchmark problems in computational aeroacoustics (CAA), NASA Conference Publication 3300, 1995.
[5] R. Hixon, Radiation and wall boundary conditions for Computational Aeroacoustics: a review, Int. J. Comput. Fluid Dyn. 18 (2004) 523–531.
[6] R. Hixon, Prefactored small-stencil compact schemes, J. Comput. Phys. 165 (2000) 522–541.
[7] R. Hixon, V. Allampali, N. Nallasamy, S. Sawyer, High-accuracy large-step explicit Runge–Kutta (HALE–RK) schemes for computational aeroacoustics, AIAA Paper 2006-0797, 2006.
[8] R. Hixon, S.-H. Shih, R.R. Mankbadi, Evaluation of boundary conditions for Computational Aeroacoustics, AIAA J. 33 (1995) 2012.
[9] R. Hixon, E. Turkel, Compact implicit MacCormack-type schemes with high accuracy, J. Comput. Phys. 158 (2000) 51–70.
[10] F.Q. Hu, Absorbing boundary conditions, Int. J. Comput. Fluid Dyn. 18 (2004) 513–552.
[11] F.Q. Hu, M.Y. Hussaini, J.L. Manthey, Low-dissipation and -dispersion Runge–Kutta schemes for Computational Acoustics, J. Comput. Phys. 124 (1996) 177–191.
[12] C.A. Kennedy, M.H. Carpenter, Several new numerical methods for compressible shear-layer simulations, Appl. Numer. Simulat. (1997).
[13] J.W. Kim, D.J. Lee, Optimized compact finite difference schemes with maximum resolution, AIAA J. 34 (5) (1996) 887–893.
[14] K.A. Kurbatskii, R.R. Mankbadi, Review of Computational Aeroacoustics algorithms, Int. J. Comput. Fluid Dyn. 18 (2004) 533–546.
[15] S.K. Lele, Compact finite difference schemes with spectral-like resolution, J. Comput. Phys. 103 (1992) 16–42.
[16] Y. Li, Wave-number extended high-order upwind-biased finite-difference schemes for convective scalar transport, J. Comput. Phys. 133 (1997) 235–255.
[17] R.K. Lin, Tony W.H. Sheu, Application of dispersion-relation-preserving theory to develop a two-dimensional convection-diffusion scheme, J. Comput. Phys. 208 (2005) 493–526.
[18] K. Mahesh, A family of high order finite difference schemes with good spectral resolution, J. Comput. Phys. 145 (1998) 332–358.
[19] A. Sescu, R. Hixon, A.A. Afjeh, Anisotropy correction of two dimensional finite difference schemes for computational aeroacoustics, AIAA Paper 2007-3495, 2007.
[20] A. Sescu, R. Hixon, A.A. Afjeh, Optimized finite difference schemes for multi-dimensional wave propagation, AIAA Paper 2007-4585, 2007.
[21] C.K.W. Tam, Computational Aeroacoustics: an overview of computational challenges and applications, Int. J. Comput. Fluid Dyn. 18 (2004) 547–567.
[22] C.K.W. Tam, J.C. Webb, Dispersion-relation-preserving finite difference schemes for Computational Aeroacoustics, J. Comput. Phys. 107 (1993) 262–281.

[23] C.K.W. Tam, J.C. Webb, Radiation boundary condition and anisotropy correction for finite difference solutions of the Helmholtz equation, J. Comput. Phys. 113 (1994) 122–133.
[24] L.N. Trefethen, Group velocity in finite difference schemes, SIAM Rev. 24 (1982) 113.
[25] R. Vichnevetsky and J.B. Bowles, Fourier analysis of numerical approximations of hyperbolic equations, SIAM Studies in Applied Mathematics, Philadelphia, 1982.
[26] F. Xiao, X.H. Tang, X.J. Zhang, Comparison of Taylor finite difference and window finite difference and their application in FDTD, J. Comput. Phys. 193 (2006) 516–534.
[27] D.W. Zingg, H. Lomax, Finite difference schemes on regular triangular grids, J. Comput. Phys. 108 (1993) 306–313.